Methods for FMCW radar map georeferencing

Marion Jaud, R. Rouveure, P. Faure, M.O. Monod

Published in *ISPRS Journal of Photogrammetry and Remote Sensing* 84 (2013) 33-42
http://dx.doi.org/10.1016/j.isprsjprs.2013.07.002

Methods for FMCW radar map georeferencing

M. Jaud*, R. Rouveure*, P. Faure, M-O. Monod

Affiliation: Irstea, UR TSCF, 9 avenue Blaise Pascal – CS 20085, F-63178 Aubière, France.
** Corresponding authors: marion.jaud@irstea.fr (+33473440711); raphael.rouveure@irstea.fr*

Abstract

In a context of mobile environment mapping, a vehicle-based radar system, K2Pi, has been developed. A mapping of the environment is carried out from the radar datasets. Given the specificities of radar maps, the main problem at this stage is to find a method to georeference these maps. This article proposes three radar map georeferencing methods. The first method is a typical manual selection of a set of control point pairs. The second method consists of matching the relative trajectory computed by a specific radar algorithm with a trajectory recorded from absolute DGPS recording. Finally, the third method, inspired by the image-to-image approach, is based on Fourier-Mellin transform which automatically registers the radar map with respect to a georeferenced aerial photograph. Successfully tested on radar datasets, this method could be applied to many other types of data.

Keywords: radar mapping; georeferencing; geolocation; Fourier-Mellin registration

1. Introduction

Microwave radar seems to be able to take up the challenge of perception in outdoor environments, covering a long range, allowing rapid collection of data and overcoming the limitations of vision-based sensors which can be affected by ambient lighting conditions, rain or dust (Peynot et al., 2010; Reina et al., 2011). Currently, radar perception systems meet requirements for new applications such as in agriculture (Noyman and Shmulevich, 1996), civil engineering (Bryson et al., 2005) and rescue (Marques et al., 2006). For such applications, the radar equipment must be small-sized, easy to load onto a vehicle and, as far as possible, inexpensive.

The ultimate aim of radar mapping is to establish the position of natural or artificial features. This generally implies data georeferencing, i.e. defining data location using map coordinates and assigning a local, regional or global coordinate reference system (Maling, 1991; Meyer, 2010). In recent years, with an increasingly fine resolution of data (sub-meter level), rapid and precise georeferencing has become a central issue. Indeed, data georeferencing allows radar data to be viewed, manipulated and analyzed with other geographic data and also to be added as a layer in a Geographic Information System (GIS). Moreover, a common referencing system enables coordinate conversion from one system to another, making for easier data exchange, comparison and combination in GIS.

Several authors have proposed procedures to obtain accurate image georeferencing. The commonly used process is based on the "manual or semi-automatic identification of control point pairs" (Toutin and Chénier, 2004; Brovelli et al., 2012; Gomez-Candon et al., 2013). These control point pairs link location on a raster image either with Ground Control Points (GCPs) measured by GPS or with GCPs on a georeferenced image or map. These GCPs are characteristic features and/or artificial targets. For mobile mapping systems, "direct georeferencing" is now widely accepted (Schwarz et al., 1993; Legat, 2006). This approach is based on determining the exterior orientation parameters with an integrated GPS/INS system (Grejner-Brzezinska, 1999). "Automatic image-to-image matching" as an alternative for indirect georeferencing has already been widely studied (Ali and Clausi, 2002; Zavorin and Le Moigne, 2005; Le Moigne et al., 2006; Brooker, 2007; Oh et al., 2011). Image registration is generally based on feature extraction in both images in order to recover the transformation parameters that describe how an image maps to another. Wong and Clausi (2007) list most of the practical problems that must be overcome with this method.

The paper is organized as follows. In section 2, we present the vehicle-based K2Pi radar system, and the mapping algorithm we have developed. The existing above-mentioned methods are tested in georeferencing the relative radar maps provided by the K2Pi system. In section 3 we describe the traditional image registration technique based on manual GCPs selection. A second method presented in section 4 of this paper takes advantage of absolute positions recorded during the path with a Differential-GPS (DGPS) by combining them with the relative radar trajectory. But, for surveys from a ground-vehicle, in many areas the DGPS can be momentarily unavailable. So an automatic indirect georeferencing is needed. An alternative method is proposed in section 5 of this article, based on Fourier-Mellin transform, which consists of automatically matching the radar map to a georeferenced orthophotograph.

In this paper an example of each method is given with a radar dataset acquired from the same residential area. The radar equipment is loaded on the top of an all-terrain vehicle. The height remains almost constant during the path. The acquisition is performed without any preparation of the study area, and in particular without arranging targets. The presented results have been georeferenced in Lambert 93, the French official coordinate system, based on GRS 80 ellipsoid.

The georeferenced orthophotograph comes from the BD ORTHO® database of IGN (French National Geographical Institute), available for the entire French territory at 50cm resolution which is updated every 5 years.

2. Description of K2Pi radar mapping

The K2Pi microwave radar equipment uses the Frequency Modulated Continuous Wave (FMCW) principle as described in details in (Monod, 1995; Rouveure et al., 2008; Rouveure et al., 2009). It can be easily loaded onto different mobile platforms, as illustrated in Fig.1a and b. The radar range is 100 m with a transmitted power about 50 mW. In one second the radar antenna achieves a complete 360° scan in the horizontal plane around the vehicle providing a so-called "panoramic radar image". This image is computed from power spectra measured at each degree of antenna rotation. By combining successive panoramic images a radar map is built as shown in Fig. 1c.

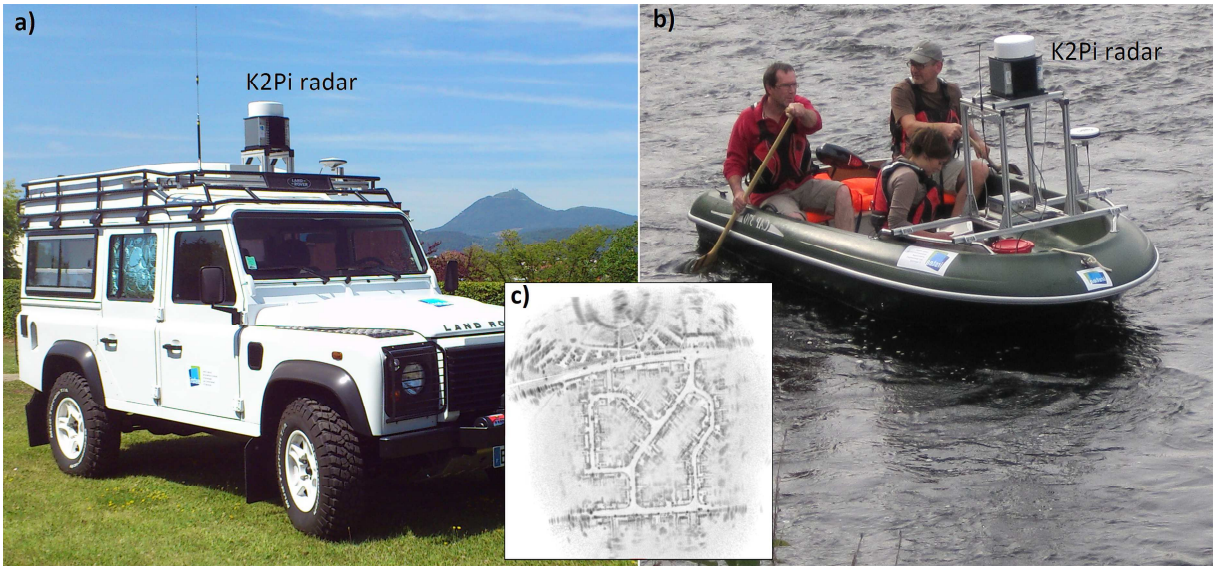

Figure 1: *Some examples of implementation of K2Pi radar system: (a) loaded on an all-terrain vehicle and (b) on a boat. (c) example of radar map. (photo Irstea©).*

In order to build consistent panoramic radar images, two kinds of corrections are applied. The first is a vehicle motion correction. Considering the antenna rotation (1 revolution per second) and the vehicle motion (translational and rotational), one would observe intra-scan distortions within the panoramic radar images. An odometer and a gyrometer are used to measure respectively the longitudinal displacement and the rotation of the vehicle. Following (Vivet et al., 2010), these measurements allow correction of the power spectra which are then projected into a reference system centered on the radar. The second kind of correction involves radar speckle. Speckle appears as a grainy "salt and pepper" texture in the image. This is caused by random constructive and destructive interferences from the multiple scattering returns that will occur within each radar resolution cell. This speckle effect is reduced through a multi-look processing phase.

The global map is built gradually by associating successive panoramic radar images thanks to the R-SLAM algorithm, as reported in (Rouveure et al., 2008). This algorithm, implemented in *Matlab®*, is based on the Simultaneous Localization And Mapping (SLAM) process, widely used in mobile robotics. This algorithm enables a sensor on board a moving vehicle to build up a relative map of its environment and simultaneously localize within this map (Durrant-Whyte and Bailey, 2006; Bailey and Durrant-Whyte, 2006). Thus, the map is built step by step, independently of the platform dynamics or of the radar position on the vehicle. The global radar map is a gray-scale raster resulting from the amplitude of the reflected echoes from the environment. The spatial resolution is 20 cm. The radar map is associated with the relative radar trajectory (called the "R-SLAM trajectory" in section 4), which is simultaneously computed.

3. Method 1: georeferencing based on tie point selection

This classic method is based on using GIS software to align the relative radar map to an existing spatial dataset in the desired map coordinate systems: e.g. topographic map, cadaster or georeferenced orthophotograph.

This process involves identifying coincident points, called “tie points” or “control points”. A tie point delivers a point location in two coordinate spaces: data coordinates and map reference (here, Lambert 93 coordinates). The georeferencing presented in Fig. 2 was carried out in *ArcGIS*® software. Tie points are landmarks, manually chosen in places that can be accurately identified both on the radar dataset and on the georeferenced orthophotograph such as corners of buildings, road intersections, etc. In this way, a list of tie points is established both in the radar map (pixel coordinates) and in the real-world coordinates (Lambert 93 coordinates). From this list of tie point coordinates *ArcGIS*® computes the default affine transformation. The number of available tie points is often limited by the poor similarity between the radar dataset and the orthophotograph.

The affine transformation (first order polynomial) is used to rotate, scale, shift and if necessary shear the radar dataset. This transformation preserves straight lines and ratios of distances between points lying on a straight line, but it does not necessarily preserve angles or lengths. For each pixel (x,y) of the original radar map, the corresponding pixel (u,v) in the projected map is computed by:

$$[u \;\; v] = [x \;\; y \;\; 1] * \begin{bmatrix} A & D \\ B & E \\ C & F \end{bmatrix} \qquad (1)$$

where *A, B, C, D, E* and *F* are unknown coefficients to compute.

The transformation parameters result from the best fit between the source and destination control points (Fig. 2). For such a transformation, a minimum of three pairs of coincident points is needed.

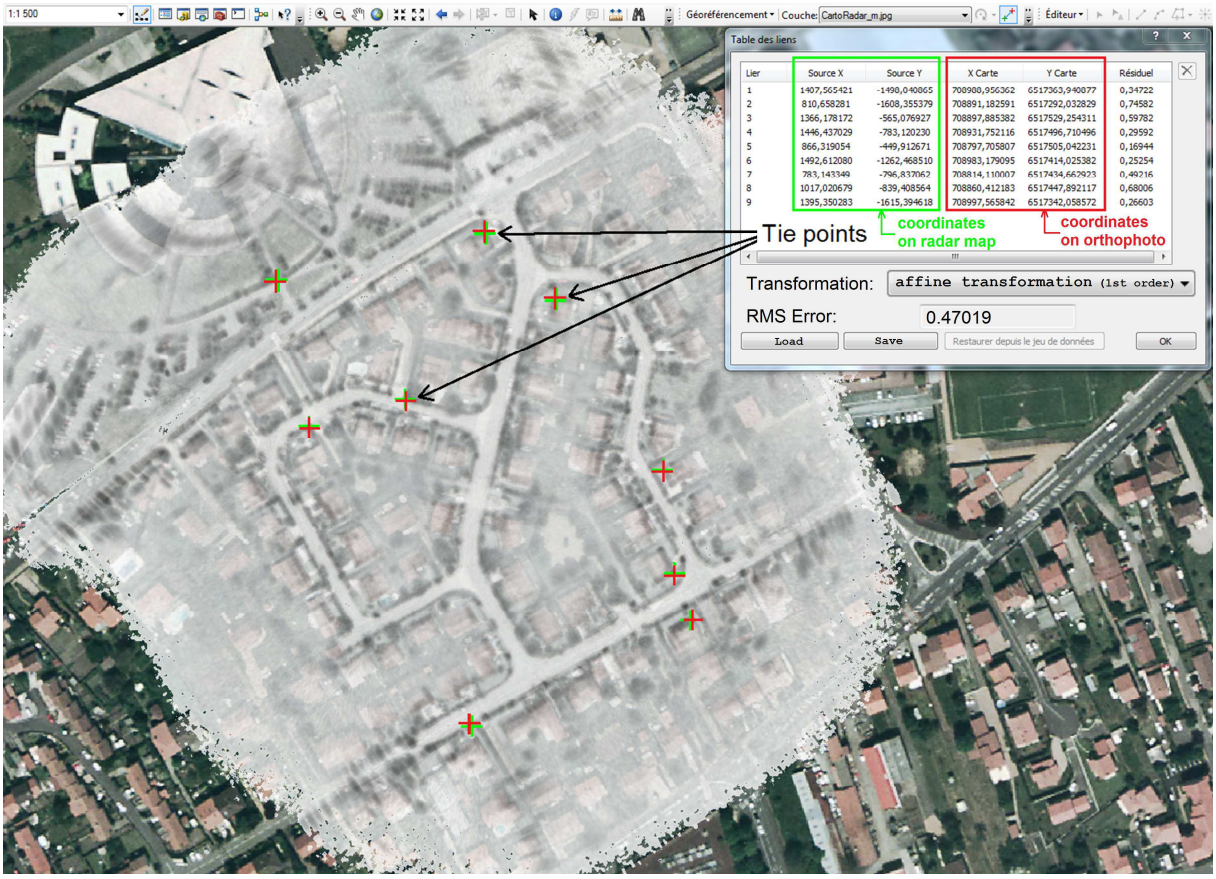

Figure 2: *Result of georeferencing with an affine transformation. Green crosses correspond to point locations on the projected radar map, whereas red crosses are their corresponding points on the orthophotograph. Background orthophotograph is extracted from BD ORTHO® (©IGN – Paris – 2004).*

For this method of georeferencing, the residual error of each pair of control points is equivalent to the Euclidean distance between the projected radar map control points (green crosses in Fig. 2) and the true location of control points picked on the orthophotograph (red crosses in Fig. 2). The total error is computed by taking the root mean square (RMS) deviation of all residual errors. If tie points are distributed all over the map, this RMS error is a good assessment of the global accuracy of the georeferencing.

For the dataset presented here, the RMS error is 0.5 m with twenty tie points. This RMS error can be affected by the choice of the control points selected by the operator (the number and spread of the tie points, precision of pointing, etc.). As the radar map resolution is nearly 20 cm and the orthophoto resolution is 50 cm, it is difficult to achieve a high level of accuracy when picking the points.

4. Method 2: trajectory matching

A second method for georeferencing radar maps has been implemented in *Matlab®*, making use of a DGPS dataset. For the dataset presented here, the vehicle was equipped with an *Ashtech®* antenna and an *Astech ProFlex 500®* receiver. The differential corrections were provided by a permanent GNSS network station, situated only 700 m distant from the acquisition zone. Throughout the over 1 km long acquisition session in an urban area, the vehicle path was measured by DGPS (Fig. 3a) at the rate of one position per second with centimetric accuracy. Simultaneously its relative displacement was estimated by the "R-SLAM trajectory" (Fig. 3b) built thanks to the R-SLAM algorithm.

The purpose of this method is to make relative R-SLAM and absolute DGPS trajectories match (Fig. 3c). To do that, each trajectory is considered as a set of tie points. A first set of transformation parameters is then roughly inferred by minimization of the residual distances between the projected tie points of the R-SLAM trajectory and the DGPS trajectory. At this stage, a slight gap may remain between these two trajectories. Indeed, the tie point pairs may be mismatched, particularly because of problems of poor synchronization. To refine the transformation parameters, the points are re-matched. At this time, each point of the transformed R-SLAM trajectory is matched to the nearest point of the DGPS trajectory. A second set of transformation parameters is inferred by minimization. The transformation matrix is built up and the whole radar map is warped (Fig. 3d). The georeferencing file is built as previously.

The computed transformations are usually similarities, but if the result is not satisfactory because of slight radar map distortions, in *Matlab®* the operator can easily replace the similarity transformation with a higher-order polynomial transformation. For a similarity, transformation parameters to determine are: a rotation, a scaling and a translation. Shapes and angles are preserved, parallel lines remain parallel, straight lines remain straight. For each pixel (x,y) of the original radar map, the corresponding pixel (u,v) in the projected map is computed by:

$$[u \;\; v] = [x \;\; y \;\; 1] * \begin{bmatrix} s\cos(\alpha) & -s\sin(\alpha) \\ s\sin(\alpha) & s\cos(\alpha) \\ Tx & Ty \end{bmatrix} \quad (2)$$

Where s is the scale factor, α the angle of rotation and T_x, T_y are respectively x and y translations. At least two control point pairs are needed to solve for the four unknown coefficients: s, α, T_x and T_y.

With such a method, errors due to poorly entered control points are avoided. This method even works with local losses of DGPS signal. Nevertheless, in cases of permanent loss of GPS signal (e.g. in forest-covered areas, urban canyons etc.), this method will fail. It may therefore be necessary to consider another approach to georeference radar maps.

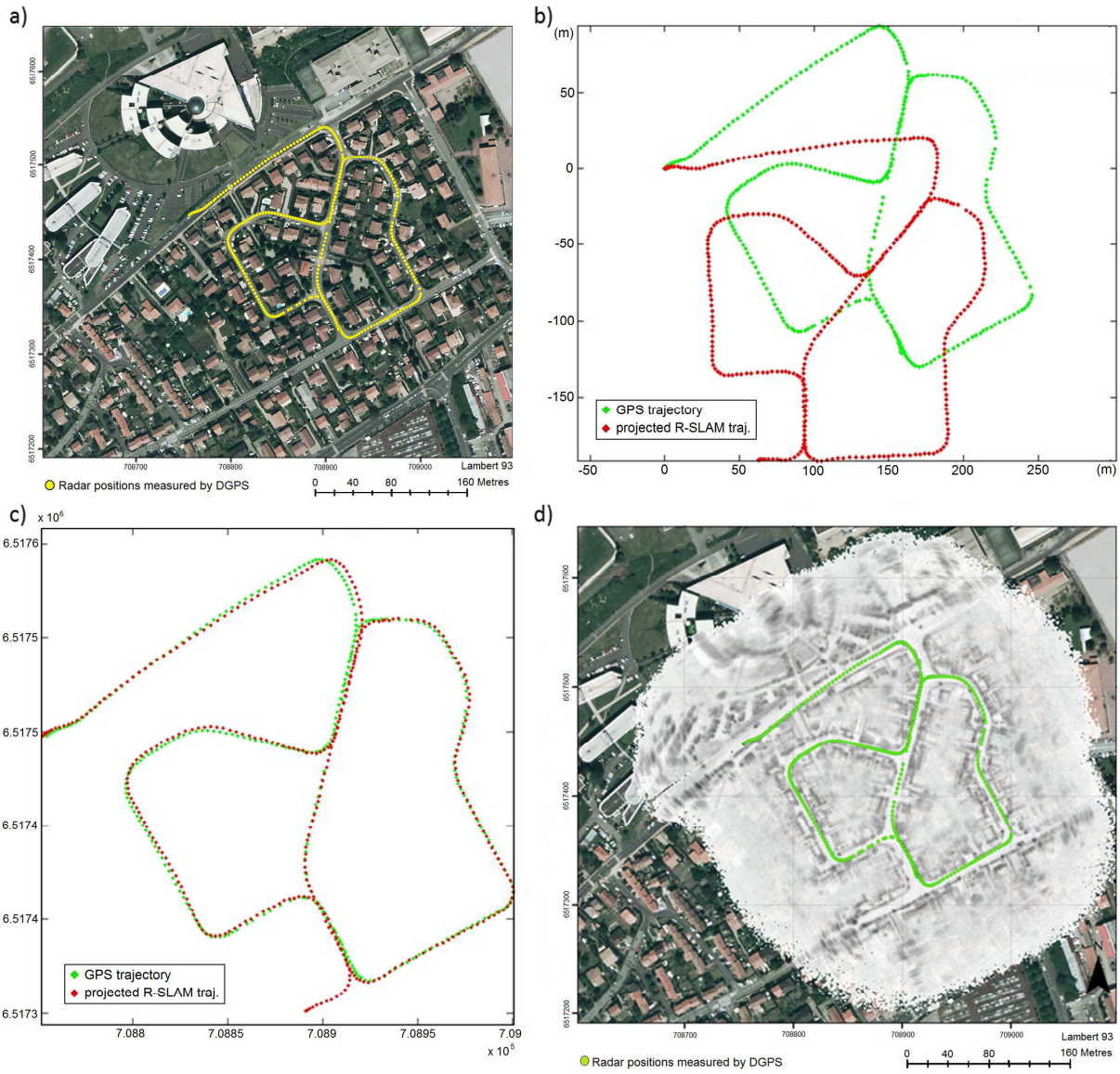

Figure 3: *Principle of georeferencing via DGPS recording.*

- *a) Vehicle path measured by DGPS (1 point/sec.) (Background extracted from BD ORTHO® - ©IGN – Paris – 2004).*
- *b) Comparison in an arbitrary bench mark of the relative R-SLAM trajectory (red) and the absolute DGPS trajectory (green) over 1km long.*
- *c) Superimposition of the projected R-SLAM trajectory (red) and the DGPS trajectory (green).*
- *d) Georeferenced radar map added in a GIS.*

5. Method 3: Fourier-Mellin registration

At first sight a radar map looks like an aerial photograph, but in detail it is very different in visible features, shape, intensity, etc. (Brooker, 2007). Thus, point feature extraction or edge extraction seems to be unfeasible to perform an image-to-image matching. A specific method based on the global similarity between the datasets has to be developed.

The main idea of this method is to carry out global image recognition between the radar map and the orthophotograph. That is to say identifying the zone covered by the radar map in a larger georeferenced orthophotograph.

The selected method is based on a Fourier-Mellin registration, which is presented in the following section (5.1). A considerable amount of literature has been published on Fourier-Mellin registration (Sheng and Arsenault, 1986; Reddy and Chatterji, 1996; Stricker, 2001). However, most of these studies only deal with registration of very similar images, generally acquired with the same sensor and with the same geometry of acquisition. Indeed, such an approach involves like-looking input images. And yet in our case, radar datasets and aerial photographs differ a lot. So image preprocessing is required. This preprocessing chain is described in Section 5.2. Results of the matching processing chain are presented in Section 5.3.

5.1- Principle of the Fourier-Mellin method

Fourier-Mellin transformation is a global rigid transformation, based on the global similarity between images. It is particularly suited to recover scale, rotation and translation parameters between two images $I_1(x,y)$ and $I_2(x,y)$ (Casasent and Psaltis, 1976; Reddy and Chatterji, 1996; Keller et al., 2005). I_1 is the "target image" and I_2 the image to align with I_1. I_2 differs from I_1 by a similarity transformation. The block-diagram of Fig. 4 sums up this transformation.

Considering that I_2 is translated, rotated and scaled compared to I_1, with a translation $T(T_x,T_y)$, a rotation $R(\theta_0)$ of angle θ_0, a scaling $S(a)$ of factor a, then

$$I_2(x,y) = a\, I_1\left(x\cos\theta_0 + y\sin\theta_0 - T_x\,, -x\sin\theta_0 + y\cos\theta_0 - T_y\right) \quad (3)$$

The first step of the Fourier-Mellin method consists of forming the magnitude of the Fourier transform of the input images I_1 and I_2 and centering on the zero frequency component. According to the Fourier translation and rotation properties, the magnitude of the Fourier transform of Eq. (3) is given by:

$$|F_2(\xi,\eta)| = \frac{1}{a^2}\, F_1\left(\frac{1}{a}(\xi\cos\theta_0 + \eta\sin\theta_0)\,, \frac{1}{a}(-\xi\sin\theta_0 + \eta\cos\theta_0)\right) \quad (4)$$

where F_1, F_2 are respective Fourier transforms of I_1 and I_2.

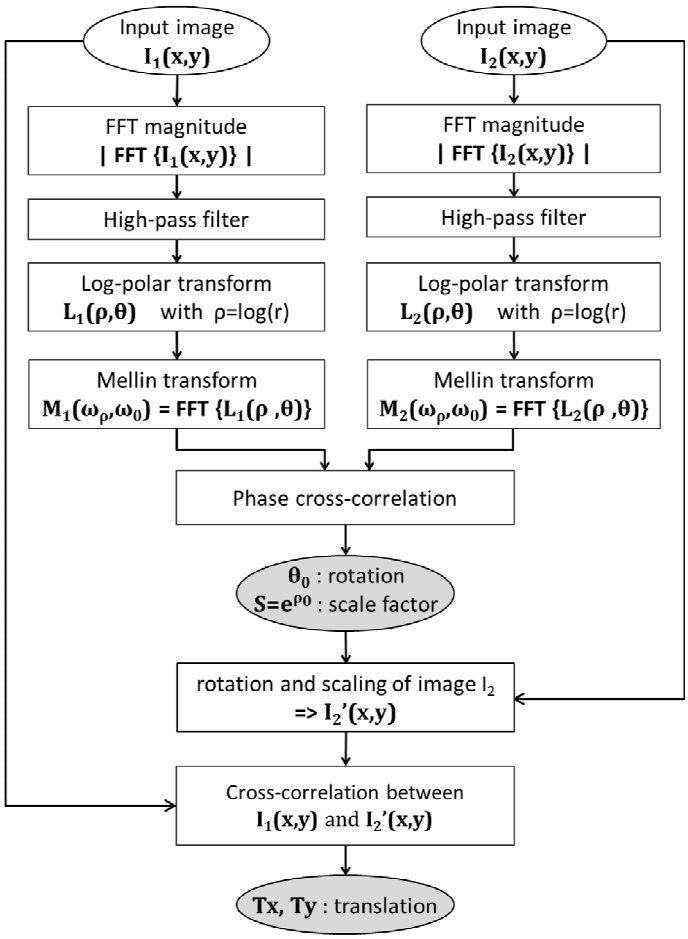

Figure 4: *Principle of the Fourier-Mellin method (FFT denotes Fast Fourier Transform) allowing computation of rotation, scaling and translation.*

Then a log-polar transformation of the spectrum is performed. This consists of a change from Cartesian image coordinates (ξ,η) into log-polar coordinates (ρ,θ), with:

$$\begin{cases} r = \sqrt{\xi^2 + \eta^2} \\ \rho = \log(r) \\ \theta = \operatorname{atan}(\eta/\xi) \end{cases} \quad (5)$$

Introducing the change in the coordinate system described in Eq. (5), Eq. (4) becomes:

$$L_2(\theta,\rho) = (1/a^2) \times L_1\left(\theta - \theta_0, \rho - \log(a)\right) \quad (6)$$

An image rotation results in a shift along the angular axis, whereas a scaling corresponds to a shift in the radial coordinates.

The next Fourier transform of L_1 and L_2 is now a 2D-transform in ρ and in θ. The resultant functions are Mellin transforms in $r = exp(\rho)$ and thus denoted M_1 and M_2:

$$M_2(\omega_\theta,\omega_\rho) = M_1(\omega_\theta,\omega_\rho)\exp\left(-j\left(\omega_\theta\theta_0 + \omega_\rho log(a)\right)\right) \quad (7)$$

The phase-difference matrix is computed and a phase-correlation is carried out. The rotation θ_0 and the scale factor $log(a)$ are deduced from the correlation peak position.

Because of the symmetry properties of the Fourier-Mellin transform, rotation is affected by a 180° ambiguity. Therefore, two cases have to be tested: $R(\theta_0)$ and $R(\theta_0+180°)$. The hypothesis related to

the highest correlation peak is chosen as the result. I_2 input image is rotated and scaled with the so calculated parameters θ_0 and a, resulting in the $I_2'(x,y)$ image.
By forming the magnitude of the Fourier Transform in the initial step (Eq. (4)) positional information is lost (Casasent and Psaltis, 1976). To retrieve it, a template-matching is performed. The template-matching is a standard approach based on cross-correlation of I_1 and I_2' in order to find the location of the elementary pattern I_2' in the large target image I_1 and to compute the translation parameters T_x and T_y.

5.2- Image preprocessing

As mentioned above, because of the dissimilarity between the two images, a preprocessing step is required. The preprocessing consists of retrieving the main common features in both images. But such an approach is not so easy, since a radar map is built from horizontal scanning of the environment, whereas an orthophoto results from vertical scanning. Moreover, multiple causes can lead to major differences between the two images: (i) features with strong radar reflectivity are not necessarily the most visible on the aerial photographs as, for example, metallic street furniture or metallic gates; (ii) both acquisitions being carried out at distinct dates, the environment is likely to have changed (reshaping, seasonal changes, etc.); (iii) aerial photographs are affected by ambient illumination conditions and can present shades which are not visible on radar maps.

The first stage consists of reducing the amount of information in both images so as to obtain two simplistic like-looking representations of the area in an urban context. In the example presented here (Fig. 5a and 6a), the most identifiable feature on both radar map and orthophotograph appears to be the roads. It is thus the feature we attempt to extract.

For the aerial photograph, the process comprises three main steps:

i) applying a color threshold and converting the result into a binary image;
ii) median filtering to reduce noise;
iii) retrieving the major boundaries to remove buildings and then applying a median filter to smooth edges.

The final result is presented in Fig. 5b.

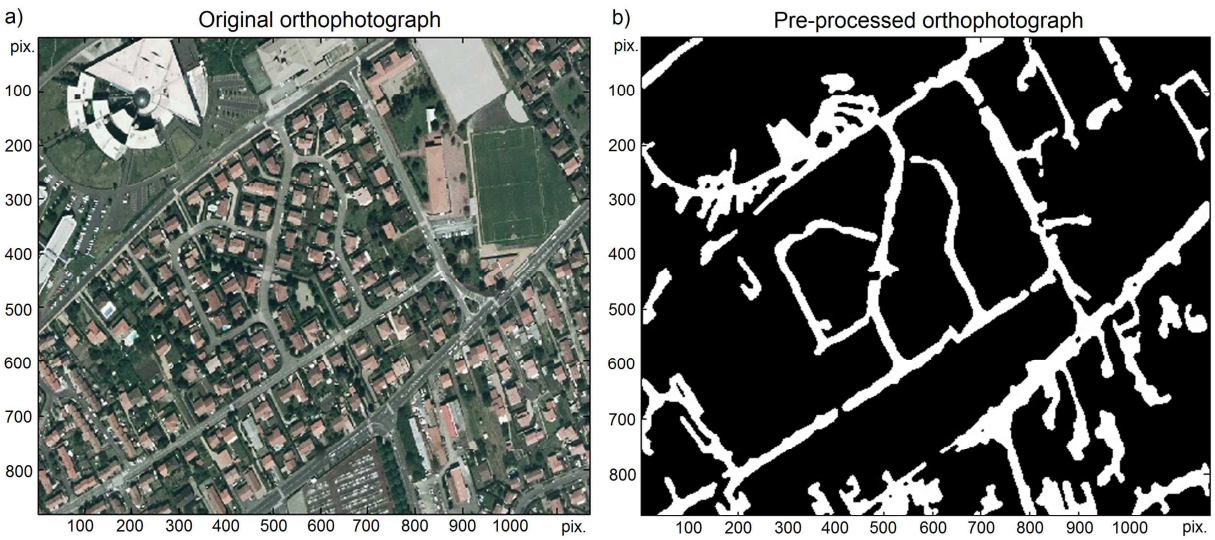

Figure 5: *Retrieval of the roads in the georeferenced orthophotograph: a) Georeferenced orthophotograph (resol.: 50cm) - extract of BD ORTHO® (©IGN Paris, 2004) ; b) Result of the processing (color thresholding, retrieval of the major boundaries and median filtering).*

For the radar map, the process is quite similar. It also comprises three main steps:

i) cropping the map to remove noisy zones and then applying a gray-level threshold and converting the result into a binary image;

ii) median filtering in order to reduce noise;

iii) retrieving the major boundaries to remove buildings and then median filtering to smooth edges.

The final result is presented in Fig. 6b.

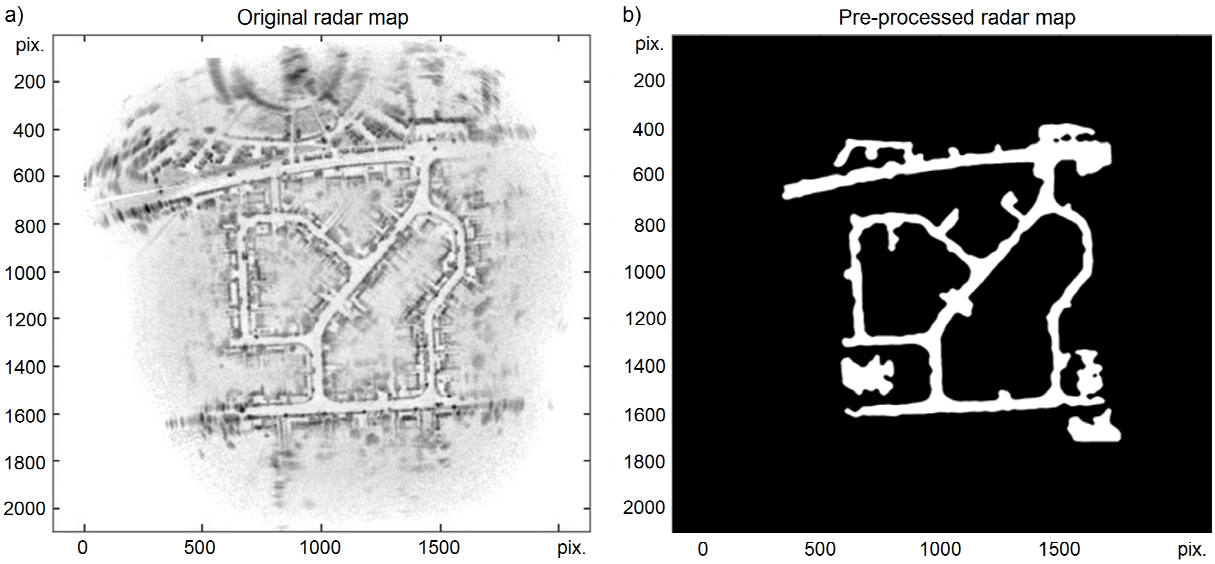

Figure 6: *Retrieval of the roads in the radar map: a) Original radar map (resol.: 20cm) ; b) Result of the processing (gray-level thresholding, retrieval of the major boundaries and median filtering).*

5.3- Matching processing chain

After the two images have been preprocessed (section 5.2), the general principle of Fourier-Mellin transform described above in section 5.1 needs to be suited to this particular application. The adapted matching process is described by the block-diagram in Fig. 7.

As the spatial resolution of both images is known (50 cm/pixel for the orthophotograph and 20 cm/pixel for the radar map), the radar map is resampled to have the same spatial resolution as the orthophotograph. Thereby the scale factor is computed beforehand, allowing a gain in processing time and increasing the robustness of the algorithm. The Fourier-Mellin method is implemented to compute the rotation and the translation. The parameters of scaling, rotation and translation obtained in this way are then applied to the original radar map and a georeferencing file is written so that the projected radar map can be added to a GIS.

This method allows automatic georeferencing independently of any GPS measurement. Its robustness is a function of the area characteristics (visibility of roads on an aerial image, dispersed or nucleated habitat, level of simplification etc.).

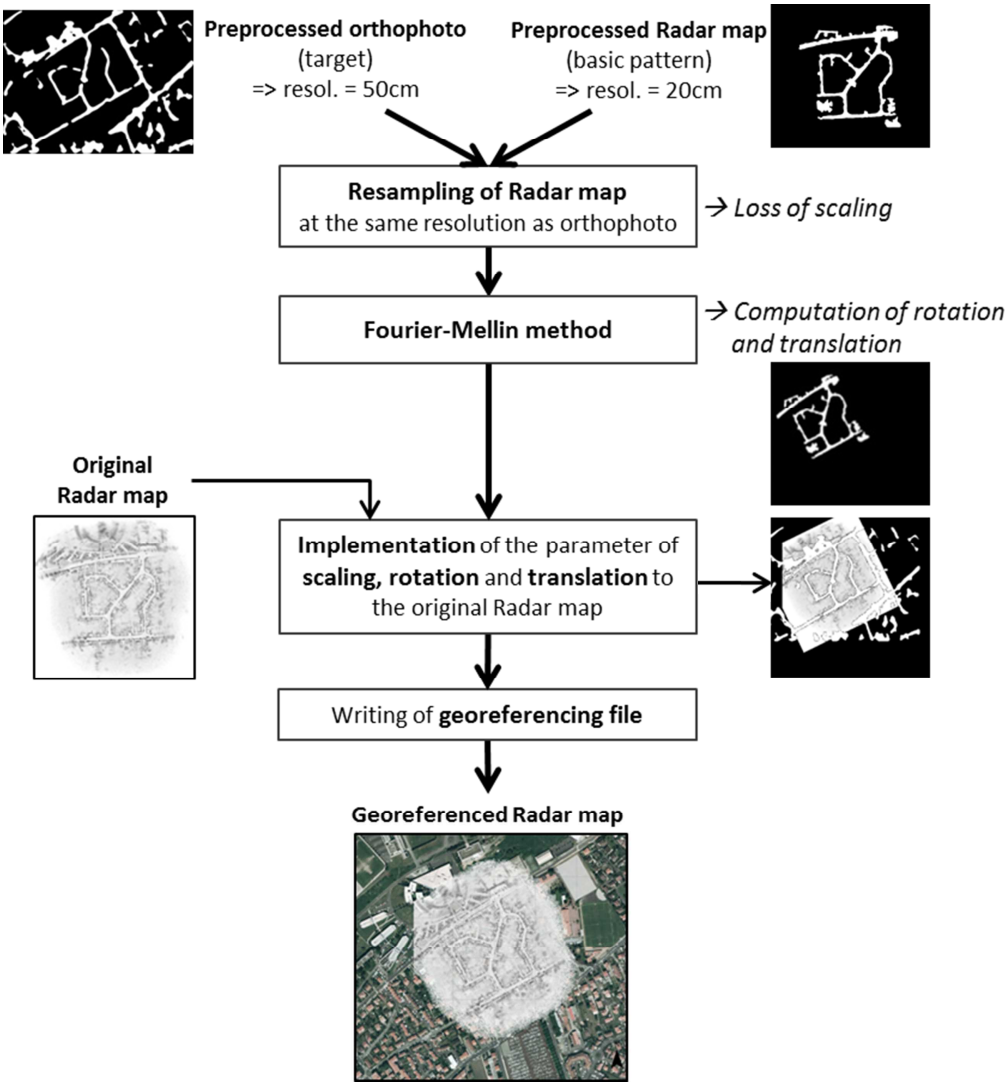

Figure 7: *Different stages of the processing chain based on the Fourier-Mellin method to match preprocessed radar map and preprocessed aerial photograph to finally georeference radar map.*

To assess the viability of the Fourier-Mellin method in different contexts, this approach has been carried out on other test areas, in more rural environments, as presented in Figs. 8 and 9. In Fig. 8 a farm is depicted with only a small section of asphalt road and different kinds of buildings: houses, barn and cattle-shed. In this case, the simplistic representation is composed of the roads and the pathways. However, the color thresholding often fails to retain only the desired identifiable features, particularly in the photograph. Indeed, if any element of the photograph (e.g. buildings) reaches the threshold, it will be taken into account in the preprocessed image and may complicate the registration.

Fig. 9 illustrates an application of the Fourier-Mellin registration in a fluvial environment. In such cases the identifiable features retained during the pre-processing step are chosen depending on the context. For example, it is relevant here to retain the river in the pre-processing step.

The global accuracy is mainly restricted by the resolution of the reference aerial photograph (in this case 50 cm) and could be improved if higher resolution ortho-images were available. However, the error of this method is not easily quantifiable since the overall image is taken into account rather than single points.

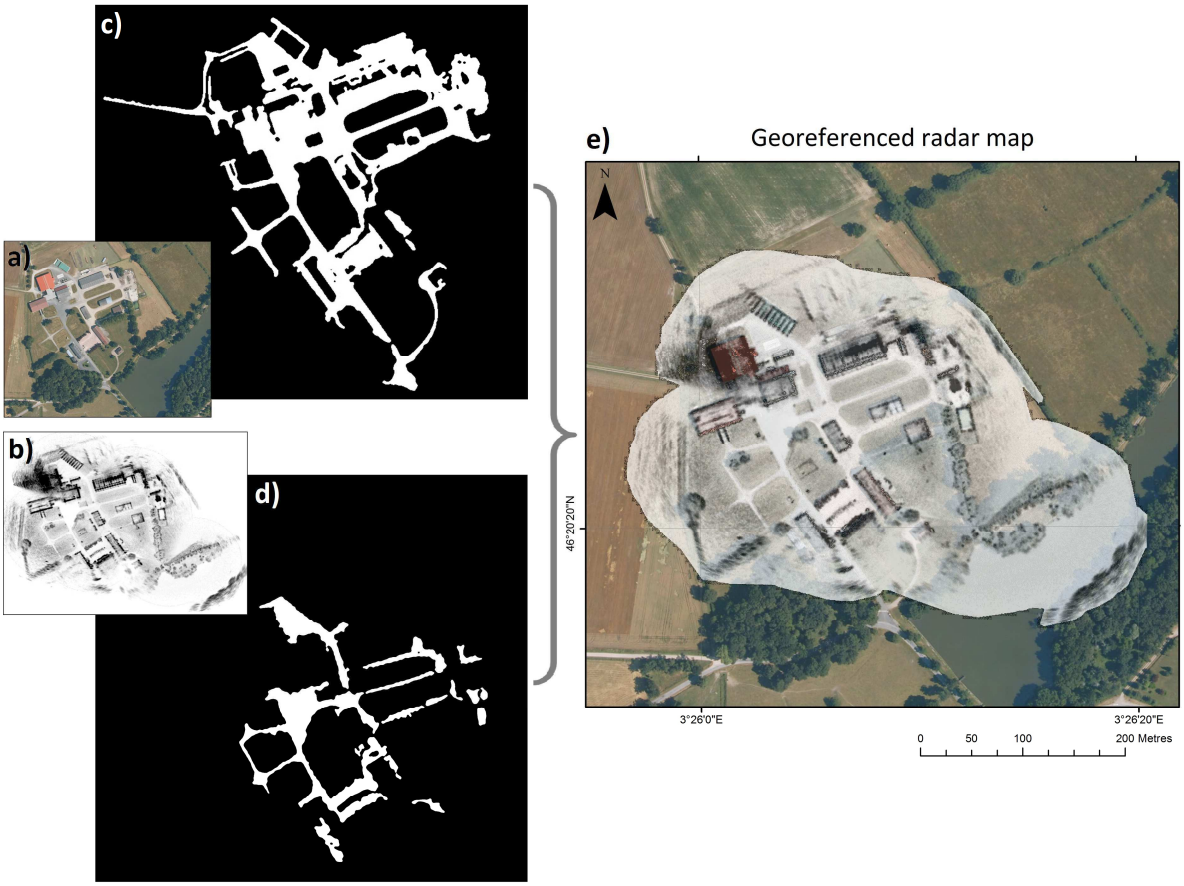

Figure 8: *Application of Fourier-Mellin registration in a rural context (farm in Montoldre, Auvergne, France). a) Georeferenced orthophotograph - extract of BD ORTHO® (©IGN Paris, 2004); b) original radar map; c) pre-processed orthophoto; d) pre-processed radar map; e) radar map georeferenced through Fourier-Mellin registration.*

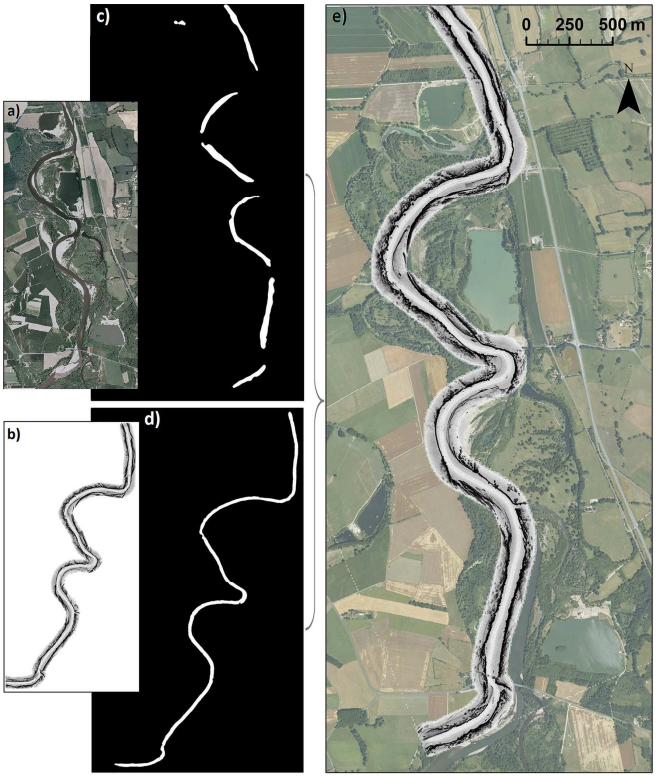

Figure 9: *Application of Fourier-Mellin registration in a fluvial context (stretch of the river Allier - Auvergne, France - 6 km long, between the confluence with the river Dore, downstream of Port de Ris, and the town of Saint Yorre). a) Georeferenced orthophotograph - extract of BD ORTHO® (©IGN Paris, 2004); b) original radar map; c) pre-processed orthophoto; d) pre-processed radar map; e) radar map georeferenced through Fourier-Mellin registration.*

6. Results and discussion

The purpose of the current study was to propose different methods of radar map georeferencing to serve as a base for future investigations. However, the main weakness of this study is the difficulty in assessing the accuracy of each method. Indeed, as the radar acquisition is performed intentionally without arranging beforehand georeferenced ground targets, it is not easy to quantify the georeferencing error.

For the estimation of this error, twenty tie points have been considered. These tie points have been used to georeference the radar map following method 1 with an affine transformation. Then the same tie points have also been picked on the projected radar maps resulting from method 2 and method 3. As method 1 is a typical georeferencing process, it will be used as the standard method to which to compare the more automated approaches. Fig. 10 shows the positions of tie points on the radar map projected by method 2 (depicted by circles), the positions of tie points on the radar map projected by method 3 (depicted by triangles) and the positions of the tie points on the radar map projected by method 1 (depicted by crosses) corresponding to the reference tie points on the orthophoto. At first sight, it seems that method 3 gives better results than method 2. It can also be noticed that the results of method 2 (depicted by circles) are not affected by an offset since the gaps change according to the position in the test area. The residual distances between each tie point series are measured. From these residuals, the RMS error is computed for each method and summarized in Table 1.

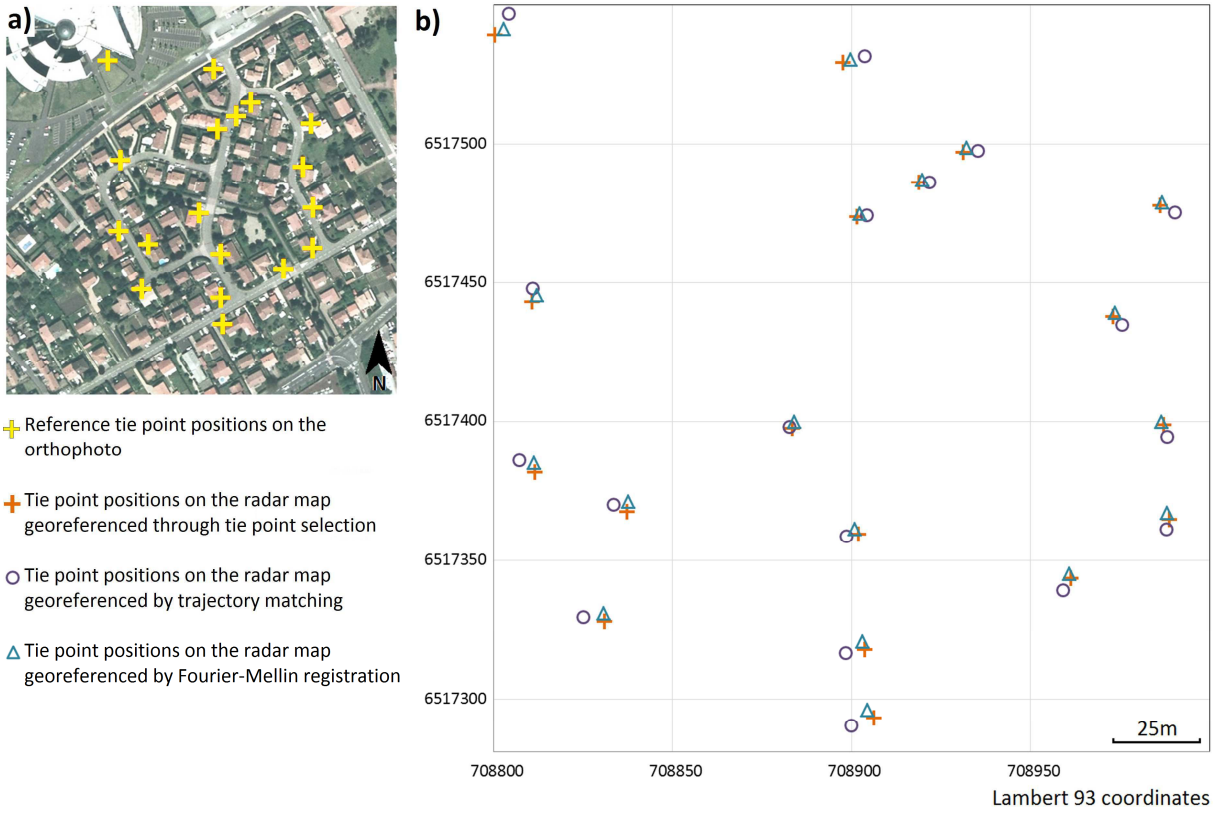

Figure 10: *a) Positions of the reference tie points on the orthophoto. b) Comparison of the results of the three georeferencing methods (see legend below Fig. 10a). Given the scale of the figure, the red crosses overlap the yellow crosses.*

Table 1: *Comparison of the different georeferencing methods.*

	Method 1	**Method 2**	**Method 3**
Requested factors	identifiable tie points	available GPS recording during the acquisition	common retrievable characteristic features
Performed transformations	affine transformation	similarity transformation	similarity transformation
RMS error (evaluated on 20 tie points)	0.50 m	1.19 m	0.62 m
Influence of the user	+	-	-
Adaptability to different study contexts	+ +	depending on availability of DGPS signal	+ / -

These results call for several possible explanations. With respect to method 1, which is based on a transformation directly computed from a list of manually selected tie points, the RMS error is mainly due to the 50 cm resolution orthophotograph. As it happens the georeferencing is at best as accurate as the data to which it is aligned. Thus the low resolution of the target image induces a decrease in georeferencing accuracy. This factor may also partly explain the RMS error of method 3.

With reference to the RMS error of methods 2 and 3, another possible explanation might be that a similarity transformation is not sufficient to project the radar map. This hypothesis suggests therefore that the dataset is slightly affected by shear distortions. In method 2 the error may also be due to: (i) a loss or a reduction in the quality of the DGPS signal, (ii) some distortions in the computed R-SLAM trajectory, (iii) the distance between locations of GPS antenna and the radar antenna on the vehicle. In order to assess more precisely the accuracy of both methods and identify the causing errors, some georeferenced radar targets will have to be added. Also taking into account the geometrical effects of relief on the radar map should most probably improve the georeferencing accuracy.

In Table 1 the main features of each method have been added in order to compare their performance but also to bring out which method would be the most suitable according to the study context. It appears that method 1 can be used in any type of environment, provided that tie points are easily identifiable. Nevertheless, the accuracy of this method is limited by the resolution of the reference image. The result is also very dependent on the selection of tie points made by the operator. In contrast, method 2 and method 3 are entirely independent of the operator. Method 2 may turn out to be very useful in areas with limited anthropization where it is difficult to identify distinctive points or characteristic features to retrieve or to use as control points. Moreover, this method does not require any reference data. Thus, the result is not affected by the quality or the age of the orthophotograph. Indeed, if the study area has undergone a major change, it can be problematic to apply methods 1 and 3.

Method 3 is fully suited to contexts where a DGPS signal is not available, for example urban canyons or river gorges. The Fourier-Mellin registration is likely to fail if the color contrast is too low or if the area has changed to the extent that no common feature can be retrieved during the pre-processing stage. By changing the threshold in the image pre-processing, it appears that the Fourier-Mellin registration can be practicable in different contexts: urban or rural environments, anthropized or not. Furthermore, it is conceivable that this approach may be used with images provided by other sensors, provided that the pre-processing stage is adapted to retrieve the most relevant common features.

7. Conclusions

FMCW vehicle-based radar may have considerable potential for mobile mapping of outdoor environments, making it possible to generate real-time 2D maps at very low cost. In order to make radar maps usable it is therefore necessary to propose a protocol for georeferencing. Considering the originality of K2Pi radar datasets, the classic methods for automatic georeferencing cannot be applied and so specific methods have been developed. Their suitability depends on the context of acquisition, such as type of environment, the presence of characteristic elements, DGPS signal quality, etc.

Apart from the classic method based on manual selection of control point pairs, two other original automatic methods have been put to the test. The trajectory matching method does not require any reference data, but needs an available DGPS signal. The third proposed method is based on Fourier-Mellin registration. From the similarity between a pre-processed orthophotograph and a pre-processed radar map, the transformation parameters are retrieved. This approach appears to be quite easily generalized to images provided by other sources.

Acknowledgements

This work is part of PELICAN Project No. ANR-2010-EMMA-033 supported by the *Agence Nationale de la Recherche*. The Project was labelled by *ViaMeca* French pole of competitiveness.

Bibliography

Ali, M.A., Clausi D.A., 2002. Automatic registration of SAR and visible band remote sensing images. Proc. IEEE Geoscience and Remote Sensing Symposium IGARSS, Toronto, 24-28 June, pp. 1331-1333.

Bailey, T., Durrant-Whyte, H., 2006. Simultaneous localization and mapping (SLAM): part II. IEEE Robotics & Automation Magazine 13 (3), 108-117.

Brooker, G.M., 2007. Correlation of Millimetre Wave Radar Images with Aerial Photographs for Autonomous Navigation of a UAV. Proc. ICST 2007 - 2nd International Conference on Sensing Technology, Palmerstone, 26-28 November, pp. 529-533.

Brovelli, M.A., Minghini M., Giori G., Beretta M., 2012. Web Geoservices and Ancient Cadastral Maps: The Web C.A.R.T.E. Project. Transactions in GIS 16 (2), 125-142.

Bryson, L.S., Maynard, C., Castro-Lacouture, D., Williams, R.L., 2005. Fully Autonomous Robot for Paving Operations. In: Tommelein, I.D. (Eds), Proc. Construction Research Congress, San Diego, 5-7 April, pp. 1-10.

Casasent, D., Psaltis, D., 1976. Position, rotation, and scale invariant optical correlation. Applied Optics 15 (7), 1795–1799.

Durrant-Whyte, H., Bailey, T., 2006. Simultaneous localization and mapping: part I. IEEE Robotics & Automation Magazine 13 (2), 99-108.

Gomez-Candon, D., Lopez-Granados F., Caballero-Novella J.J., Pena-Barragan J.M., Gomez-Casero M.T., Jurado-Exposito M., Garcia-Torres L., 2013. Semiautomatic Detection of Artificial Terrestrial Targets for Remotely Sensed Image Georeferencing. IEEE Geoscience and Remote Sensing Letters 10 (1), 184-188.

Grejner-Brzezinska, D.A., 1999. Direct Exterior Orientation of Airborne Imagery with GPS/INS System: Performance Analysis. Navigation 46 (4), 261-270.

Keller, Y., Averbuch, A., Israeli, M., 2005. Pseudopolar-based estimation of large translations, rotations, and scalings in images. IEEE Transactions on Image Processing 14 (1), 12-22.

Legat, K., 2006. Approximate direct georeferencing in national coordinates. ISPRS Journal of Photogrammetry and Remote Sensing 60 (4), 239-255.

Le Moigne, J., Cole-Rhodes, A., Eastman, R., Jain, P., Joshua, A., Memarsadeghi, N., Mount, D., Netanyahu, N., Morisette, J., Uko-Ozoro, E., 2006. Image Registration and Fusion Studies for the Integration of Multiple Remote Sensing Data. Proc. 2006 IEEE International Conference Acoustics, Speech and Signal Processing ICASSP, Toulouse, 14-19 May, pp. 1189-1192.

Maling, D.H., 1991. Coordinates Systems and Map Projections for GIS. In: Maguire, D.J., Goodchild, M.F., Rhind, D.W. (Eds), Geographical Information Systems: Principles and Applications, London, pp. 135-146.

Marques, C., Cristóvão, J., Lima, P., Frazão, J., Ribeiro, I., Ventura, R., 2006. Raposa: Semi-autonomous robot for rescue operations. Proc. IEEE/RSJ International Conference on Intelligent Robots and Systems, Beijing, 9-15 October, pp. 3988-3993.

Meyer, T.H., 2010. Introduction to geometrical and physical geodesy: foundations of geomatics, first ed. ESRI Press, Redlands.

Monod, M.O., 1995. Frequency modulated radar: a new sensor for natural environment and mobile robotics. Ph.D. Thesis, Paris VI University, France.

Noyman, Y., Shmulevich, I., 1996. Ground surface sensing through plant foliage using an FM-CW radar. Computers and Electronics in Agriculture 15 (3), 181-193.

Oh, J., Toth, C.K., Grejner-Brzezinska, D.A., 2011. Automatic Georeferencing of Aerial Images Using Stereo High-Resolution Satellite Images. Photogrammetric Engineering and Remote Sensing 77 (11), 1157-1168.

Peynot, T., Scheding, S., Terho, S., 2010. The Marulan Data Sets: Multi-Sensor Perception in Natural Environment with challenging conditions. The International Journal of Robotics Research 29 (13), 1602-1607.

Reddy, B.S., Chatterji, B.N., 1996. An FFT-based technique for translation, rotation, and scale-invariant image registration. IEEE Transactions on Image Processing 5 (8), 1266-1271.

Reina, G., Underwood, J., Brooker, G., Durrant-Whyte, H., 2011. Radar-based perception for autonomous outdoor vehicles. Journal of Field Robotics 28 (6), 894-913.

Rouveure, R., Monod, M.O., Faure, P., 2008. Mapping of the environment with a high resolution ground-based radar imager. Proc. IEEE Mediterranean Electrotechnical Conference MELECON, Ajaccio, 5-7 May, pp. 801-807.

Rouveure, R., Faure, P., Monod, M.O., 2009. Radar Imager for Perception and Mapping in Outdoor Environments. Proc. International Conference on Advanced Concepts for Intelligent Vision Systems ACIVS, Bordeaux, 28 September - 2 October, pp. 618-628.

Schwarz, K.P., Chapman, M.A., Cannon, M.E., Gong, P., 1993. An integrated INS/GPS approach to the georeferencing of remotely sensed data. Photogrammetric Engineering and Remote Sensing 59 (11), 1667-1674.

Sheng, Y., Arsenault, H.H., 1986. Experiments on pattern recognition using invariant Fourier-Mellin descriptors. Journal of the Optical Society of America 3 (6), 771-776.

Stricker, D., 2001. Tracking with reference images: a real-time and markerless tracking solution for out-door augmented reality applications. Proc. Conference on Virtual Reality, Archeology, and Cultural Heritage, Glyfada, 28-30 November, pp. 77-82.

Toutin, T., Chérnier, R., 2004. GCP requirement for high-resolution satellite mapping. International Archives of Photogrammetry, Remote Sensing and Spatial Information Sciences 35 (Part 3B), 836-839.

Vivet, D., Checchin, P., Chapuis, R., 2010. Line-based SLAM with slow rotating range sensors: results and evaluations. Proc. IEEE International Conference on Control, Automation, Robotics and Vision ICARCV, Singapore, 7-10 December, pp. 423-430.

Wong, A., Clausi, D.A., 2007. ARRSI: Automatic Registration of Remote-Sensing Images. IEEE Transactions on Geoscience and Remote Sensing 45 (5), 1483-1493.

Zavorin, I., Le Moigne, J., 2005. Use of multiresolution wavelet feature pyramids for automatic registration of multisensor imagery. IEEE Transactions on Image Processing 14 (6), 770-782.